Reionization inference from the CMB optical depth and E-mode polarization power spectra

Yuxiang Qin [1]★ Vivian Poulin,[2] Andrei Mesinger [1] Bradley Greig [3,4] Steven Murray[5]
and Jaehong Park [1]

[1] *Scuola Normale Superiore, Piazza dei Cavalieri 7, I-56126 Pisa, Italy*
[2] *Laboratoire Univers & Particules de Montpellier, CNRS, Université de Montpellier, Place Eugène Bataillon, F-34095 Montpellier Cedex 05, France*
[3] *School of Physics, University of Melbourne, Parkville, VIC 3010, Australia*
[4] *ARC Centre of Excellence for All Sky Astrophysics in 3 Dimensions (ASTRO 3D), Australia*
[5] *School of Earth and Space Exploration, Arizona State University, Tempe, 85287-6004 AZ, USA*

ABSTRACT

The Epoch of Reionization (EoR) depends on the complex astrophysics governing the birth and evolution of the first galaxies and structures in the intergalactic medium. EoR models rely on cosmic microwave background (CMB) observations, and in particular the large-scale E-mode polarization power spectra (EE PS), to help constrain their highly uncertain parameters. However, rather than directly forward-modelling the EE PS, most EoR models are constrained using a summary statistic – the Thompson scattering optical depth, τ_e. Compressing CMB observations to τ_e requires adopting a basis set for the EoR history. The common choice is the unphysical, redshift-symmetric hyperbolic tangent (tan*h*) function, which differs in shape from physical EoR models based on hierarchical structure formation. Combining public EoR and CMB codes, 21CMFAST and CLASS, here we quantify how inference using the τ_e summary statistic impacts the resulting constraints on galaxy properties and EoR histories. Using the last *Planck* 2018 data release, we show that the marginalized constraints on the EoR history are more sensitive to the choice of the basis set (tan*h* versus physical model) than to the CMB likelihood statistic (τ_e versus PS). For example, EoR histories implied by the growth of structure show a small tail of partial reionization extending to higher redshifts. However, biases in inference using τ_e are negligible for the *Planck* 2018 data. Using EoR constraints from high-redshift observations including the quasar dark fraction, galaxy UV luminosity functions, and CMB EE PS, our physical model recovers $\tau_e = 0.0569^{+0.0081}_{-0.0066}$.

Key words: galaxies: high-redshift – intergalactic medium – cosmic background radiation – dark ages, reionization, first stars – early Universe – cosmology: theory.

1 INTRODUCTION

The Epoch of Reionization (EoR) leaves footprints in the observed cosmic microwave background (CMB) as the photons Thomson scatter off free electrons. These include damping the primary temperature anisotropies, inducing secondary anisotropies from the bulk motion of ionized gas (i.e. the kinetic Sunyaev–Zel'dovich effect), and prompting curl-less (i.e. E-mode) polarization from the CMB quadrupole (e.g. Sunyaev & Zeldovich 1980; Vishniac 1987; Hu 2000; Hu & Dodelson 2002; McQuinn et al. 2005; Dvorkin, Hu & Smith 2009). Of these, the large-scale E-mode polarization anisotropies are a particularly powerful probe of the EoR as they are less plagued by degeneracies and systematics (e.g. Reichardt 2016). Reionization models can therefore constrain their largely uncertain parameters that describe the ionizing emissivity of the early Universe, through forward-modelling the EE autocorrelation power spectra (PS) and comparing against measurements from the *Planck* satellite (Planck Collaboration XLVII, V 2016e, 2020a; e.g. Hu & Holder

2003; Mortonson & Hu 2008; Miranda et al. 2017; Hazra et al. 2020).

Nevertheless, most reionization models do not directly use the CMB PS to constrain their parameters. Instead, they use a summary statistic which has become one of the de-facto standard cosmological parameters – the direction-averaged Thomson scattering optical depth, τ_e. In going from the observed PS to τ_e, one needs to adopt a basis set for the EoR history – a parametrization of the redshift evolution of the comoving number density of free electrons (n_e). Early works adopted a simple step function reionization at a given redshift z_{re} (Page et al. 2007; Spergel et al. 2007). Currently, the most common choice has a hyperbolic tangent functional form (tan*h*; Lewis 2008) parametrized by a reionization mid-point (z_{re}) and a redshift duration (Δ_{re}; see equation 1). For example, the latest constraints on τ_e published by *Planck*, $\tau_e = 0.0522 \pm 0.0080$ (the TT + low*E* reconstruction in Planck Collaboration VI 2020b), were generated by fixing a width of $\Delta_{re} = 0.5$, sampling a flat prior over z_{re}, and comparing against the observed large-scale E-mode PS (and also the temperature autocorrelation).

However, the redshift-symmetric evolution given by tan*h* differs in shape from both physical and empirical models of EoR history,

★ E-mail: yuxiang.l.qin@gmail.com

based on the growth of cosmic structure and/or fit to observed galaxy luminosity functions (LFs; e.g. Choudhury & Ferrara 2006; Raskutti et al. 2012; Greig & Mesinger 2017a; Qin et al. 2017; Gorce et al. 2018; Koh & Wise 2018; Roy et al. 2018; Kulkarni et al. 2019; Qin et al. 2020). Therefore, *computing a likelihood using the τ_e summary statistic instead of directly forward-modelling the CMB PS can bias EoR model constraints* (e.g. Douspis et al. 2015; Planck Collaboration XLVII 2016e; Miranda et al. 2017; Hazra et al. 2020). For example, Miranda et al. (2017) and Heinrich & Hu (2018) claimed (though see Millea & Bouchet 2018 and Planck Collaboration VI 2020b) that the *Planck* 2015 E-mode PS prefers reionization histories with an extended tail of partial reionization towards very high redshifts ($z > 15$). This would have significant implications for our understanding of the very first galaxies. However, quantifying such claims is difficult without directly performing inference on galaxy model parameters.

In this work, we use a physically motivated EoR model to quantify how inference using the τ_e summary statistic (instead of directly forward-modelling the E-mode PS) impacts the resulting constraints on galaxy properties and EoR histories. Using the last *Planck* data release, we show that the marginalized constraints on the EoR history are far more sensitive to the choice of the basis set (tan$h$ versus physical model) than to the CMB likelihood statistic (τ_e versus PS). Specifically, we use the latest v3.0.0 release[1] (Murray et al., in preparation) of 21CMFAST (Mesinger & Furlanetto 2007; Mesinger, Furlanetto & Cen 2011), whose parametrization for galaxy properties is informed by high-redshift UV LFs (Park et al. 2019). To calculate the CMB PS for a given reionization history and compute the corresponding likelihood, we add the Cosmic Linear Anisotropy Solving System (CLASS;[2] Lesgourgues 2011) Boltzmann solver and the *Planck* likelihood codes (PLC;[3] Planck Collaboration XI, V 2016a, 2020a) to the upcoming v1.0.0 release[4] of the public 21CMMC Markov chain Monte Carlo (MCMC) framework (Greig & Mesinger 2015, 2017b). All codes developed here are publicly available.

This paper is organized as follows. We present our analysis of the *Planck* data and discuss the difference between the 2015 and 2018 results in Section 2. In Section 3, we briefly introduce our EoR model (Section 3.1) and show the resulting constraints inferred from CMB and other observations. We quantify the bias from the choice of basis set for EoR histories in Section 3.2 and the choice of likelihood statistics in Section 3.3. We summarize our results and conclusions in Section 4.

2 MODELLING CMB OBSERVABLES

CLASS (Lesgourgues 2011) computes CMB anisotropies including temperature and polarization, and calculates their autocorrelation and cross-correlation PS. In its default configuration, CLASS computes the ionization history from $z = 10^4$ and throughout recombination (e.g. via the code RECFAST; Seager, Sasselov & Scott 1999; Chluba 2010), and includes a parametrized function for the EoR history. The EoR is assumed to have the tan$h$ form as follows:

$$n_e = \frac{n_H + n_{He}}{2}\left\{1 + \tan h\left[\left(1 - \left(\frac{1+z}{1+z_{re}}\right)^{1.5}\right)\frac{1+z_{re}}{1.5\Delta_{re}}\right]\right\},\quad (1)$$

[1] https://github.com/21cmfast/21cmFAST
[2] https://github.com/lesgourg/class_public
[3] http://pla.esac.esa.int/pla
[4] https://github.com/21cmfast/21CMMC

Table 1. Revisiting the models from Miranda et al. (2017), using both *Planck* 2015 and 2018 data. The models correspond to those shown in Fig. 1; the parameters are fixed and are not allowed to vary so as to better fit the 2018 data. For each model, we list the optical depth and the difference in the reduced χ^2 with respect to the Pop-II model (computed using the *Planck* likelihood code).

Model	*Planck* 2015[a]		*Planck* 2018[b]	
	τ_e	$\chi^2 - \chi^2_{PopII}$	τ_e [c]	$\chi^2 - \chi^2_{PopII}$
tan$h$	0.0792	1.13	0.0788	−1.14
Pop-II[d]	0.0832	0	0.0827	0
Pop-III	0.0926	−0.96	0.0921	5.47
Pop-III, self-regulated	0.1049	−2.27	0.1043	16.10

Notes.[a]This column assumes cosmological parameters (i.e. the density and Hubble constant) from the $TT + lowP$ reconstruction in Planck Collaboration XIII (2016b) and calculates χ^2 using the *low_l/bflike/lowl_SMW_70_dx11d_2014_10_03_v5c_Ap* likelihood in PLC 2.0 (Planck Collaboration XI 2016a). This likelihood considers both EE, TT, TE, and BB components.
[b]Results in this column, similarly to the *Planck* 2015 column, assume cosmological parameters from the $TT + lowE$ reconstruction in Planck Collaboration VI (2020b), and use the *low_l/simall/simall_100x143_offlike5_EE_Aplanck_B* likelihood in PLC 3.0 (Planck Collaboration V 2020a). This likelihood allows users to consider only the EE PS, which is used in this work.
[c]For each model, there are slight changes in the resulting optical depth when comparing the *Planck* 2015 and 2018 columns. This is due to the variation in the Hubble constant (see equation 2) when different cosmological parameters are adopted.
[d] χ^2_{PopII}=10492.45 (407.50) for *Planck* 2015 (2018).

with n_H and n_{He} representing the average comoving number density of hydrogen and helium, respectively. Instead of using the default tan$h$ parametrization, here we forward-model the CMB observables by passing any given ionization history directly to CLASS. We then compare the theoretical PS against observations using the *Planck* likelihood codes (Planck Collaboration XI, V 2016a, 2020a; see more in Table 1). On the other hand, the integrated history of reionization can also be summarized using the Thomson scattering optical depth

$$\tau_e = \int_0^{z_d} cH^{-1}(1+z)^2 n_e\sigma_T,\quad (2)$$

where $z_d \sim 1100$, c, $H(z)$, and $\sigma_T = 6.65 \times 10^{-25}$ cm^2 are the redshift of the last scattering surface at recombination, the speed of light, the Hubble constant at redshift z, and Thomson scattering cross-section, respectively. Below we also perform EoR inference with a Gaussian likelihood ($\mathscr{L}$) computed using τ_e from *Planck* (Planck Collaboration XVI, VI 2016c, 2020b). This allows us to compare the resulting EoR parameter constraints to those obtained from using directly the EE PS for the likelihood.

2.1 Preference for an early reionization?

The mapping of CMB PS to the τ_e summary statistic depends on the chosen basis set and corresponding priors for the EoR history. The sensitivity of the resulting τ_e constraints to this choice has been debated extensively in the literature (e.g. Douspis et al. 2015; Planck Collaboration XLVII, VI 2016e, 2020b; Reichardt 2016; Heinrich, Miranda & Hu 2017; Millea & Bouchet 2018; Hazra et al. 2020). As mentioned in the introduction, using different EoR basis sets to infer τ_e from the CMB PS and then from τ_e to astrophysical parameters could result in biases.
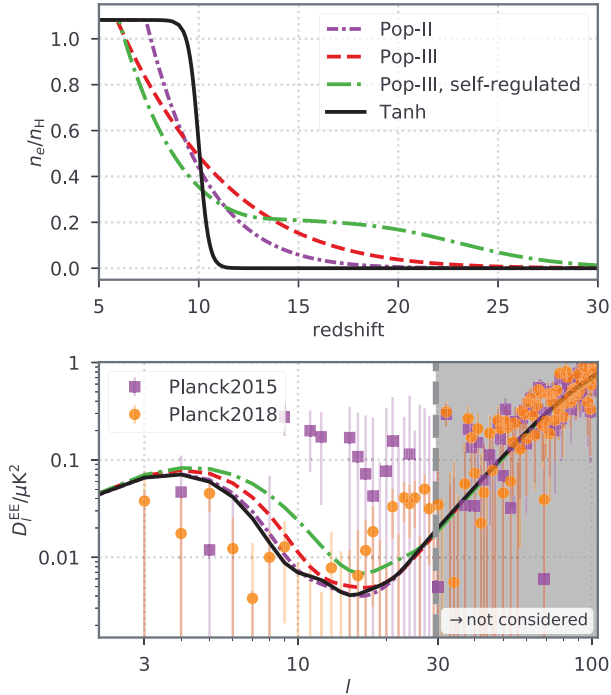
Figure 1. Reanalysing models from Miranda et al. ([2017](#)) with cosmological parameters given by the TT + low*P* reconstruction in Planck Collaboration VI ([2020b](#)). *Top panel:* The best-fitting EoR models from Miranda et al. ([2017](#)). *Bottom panel:* Corresponding PS of the E-mode polarization anisotropies with *Planck* 2015 and 2018 measurements shown as squares and circles, respectively. Only the large-scale ($2 \leq \ell \leq 29$) PS is considered when evaluating the likelihoods as these scales are most relevant for the EoR.

Constraining astrophysics directly using the CMB PS bypasses this issue. For instance, Miranda et al. ([2017](#)) adopted a simple EoR galaxy model, parametrized by the ionizing efficiencies of Pop-II or Pop-III dominated galaxies, and constrained their model parameters directly from the *Planck* 2015 (Planck Collaboration XLVII [2016e](#)) PS observations (see also Hazra et al. [2020](#)). The top panel of Fig. [1](#) shows their best-fitting models, where

(i) *Pop-II* only considers UV ionizing photons from Pop-II star-dominated galaxies;

(ii) *Pop-III* considers UV ionizing photons from both Pop-II and Pop-III star-dominated galaxies; and

(iii) *Pop-III, self-regulated* is similar to the previous model but assumes a significant contribution from Pop-III stars in the early universe ($z \sim 20$) before their formation becomes completely quenched when n_e/n_H reaches 0.2.

Also shown is a tan*h* model that assumes a fairly sharp transition at $z_{re} \sim 10$ (see equation 1). Comparing the corresponding large-scale E-mode polarization PS of these models against the *Planck* 2015 measurement (Planck Collaboration XLVII [2016e](#)), Miranda et al. ([2017](#)) concluded *Planck* 2015 might favour a significant UV ionizing photon contribution from Pop-III star-dominated galaxies in the early Universe and the resulting optical depth is much higher than what the default tan*h* parametrization suggests. This example illustrates how a reionization model informed only by the CMB optical depth could result in biased constraints, compared to using the PS directly in the inference.

2.1.1 From Planck 2015 to 2018

From their 2015 to 2018 data release, the *Planck* collaboration has made tremendous efforts in improving the characterization and removal of systematic uncertainties affecting the polarization data of the *Planck* High Frequency Instrument (HFI) on large angular scales (Planck Collaboration XLVI [2016d](#)). With such improvements, the *Planck* collaboration has shown that the mean value and uncertainties of the optical depth deduced from the low-ℓ data assuming the tan*h* EoR model have significantly decreased from $\tau = 0.078 \pm 0.010$ (the TT + low*P* reconstruction in Planck Collaboration XIII [2016b](#)) to $\tau = 0.0522 \pm 0.0080$ (TT + low*E* in Planck Collaboration VI [2020b](#)).

Before discussing the difference between EoR inference from the CMB optical depth and PS, we revisit the four best-fitting models from Miranda et al. ([2017](#)) mentioned above, using the updated measurement from *Planck* 2018 (Planck Collaboration V [2020a](#)) to see if the latest data still support an earlier reionization and larger optical depths.

We show the PS of the E-mode polarization anisotropies using the Miranda et al. ([2017](#)) EoR models in the bottom panel of Fig. [1](#) assuming *Planck* 2018 TT + low*E* cosmology (Ω_m, Ω_b, Ω_Λ, h, σ_8 = 0.321, 0.04952, 0.679, 0.6688, 0.8118; Planck Collaboration VI [2020b](#)). We present the relative $\chi^2 \equiv -2 \ln \mathscr{L}$ and the corresponding optical depth[5] in Table [1](#), together with the results using *Planck* 2015 TT + low*P* cosmology (Ω_m, Ω_b, Ω_Λ, h, σ_8 = 0.315, 0.04904, 0.685, 0.6731, 0.829; Planck Collaboration XIII [2016b](#)) for comparison. We conclude that, unlike *Planck* 2015, the 2018 measurement no longer prefers an earlier reionization or a significant contribution from Pop-III stars to early reionization – the likelihood decreases when ionization starts at earlier times (see e.g. Millea & Bouchet [2018](#)). This is mainly driven by the reduced amplitude at multipole $\ell \sim 10$–20 in the updated *Planck* E-mode PS (see the bottom panel of Fig. [1](#)). Consequently, models with a better fit to the updated PS measurement also return an optical depth closer to the reported value from Planck Collaboration VI ([2020b](#)), indicating that EoR inference biases from using the CMB optical depth might be insignificant in *Planck* 2018 (see also v2 of Hazra et al. [2020](#)).

For the remainder of the paper, we focus only on the *Planck* 2018 data. Using a flexible, physical EoR model, we forward-model the EE PS, and quantify the bias from using the τ_e summary statistic instead of the PS.

3 EOR INFERENCE FROM THE CMB

To compute the impact of realistic reionization histories on the CMB PS, we connect 21CMFAST (Mesinger & Furlanetto [2007](#); Mesinger et al. [2011](#); Murray et al., in preparation) to CLASS (Lesgourgues [2011](#)). Specifically, for a given set of cosmological and astrophysical parameters, 21CMFAST performs a 3D EoR simulation.[6] The volume-

---

[5]Note that the updated optical depths from the four models presented in Fig. [1](#) using *Planck* 2018 cosmology are all higher than the reported value (0.0522 ± 0.0080; Planck Collaboration VI [2020b](#)). This is due to the fact that the model parameters were chosen to fit the 2015 data, not the 2018. Here, we do not vary the parameters of the Miranda et al. ([2017](#)) models but instead use a different parametrization introduced below.

[6]We do not explicitly model helium reionization. Instead, we assume helium to be singly ionized following the same rate as hydrogen before becoming fully ionized at $z = 3$ (Hogan, Anderson & Rugers [1997](#); Worseck et al. [2011](#), [2016](#)).

averaged EoR history of that simulation is passed to CLASS, which then computes the corresponding CMB PS.

With this interface, we use the MCMC driver 21CMMC (Greig & Mesinger 2015, 2017b) to sample two EoR models: (i) the astrophysical galaxy-based parametrization native to 21CMFAST (see below) and (ii) the commonly used, two-parameter tan*h* model (see equation 1). In addition to varying the EoR parametrization, we also check how the inference is affected by the choice of likelihood statistic: (i) $\tau_{\rm e}$ or (ii) the EE PS. Specifically, for (i) we use $\tau_{\rm e} = 0.0522 \pm 0.0080$ from the TT + low*E* result in Planck Collaboration VI (2020b) and for (ii) we use the large-scale ($2 \leq \ell \leq 29$) E-mode polarization measurements and the likelihood from Planck Collaboration V (2020a).

3.1 Modelling the EoR

Our EoR model describes galaxy properties mostly using power-law scaling relations with respect to their host halo masses (Park et al. 2019) and calculates the 3D reionization evolution following an excursion-set approach based on the cumulative number density of ionizing photons and recombinations (e.g. Furlanetto, Zaldarriaga & Hernquist 2004; Sobacchi & Mesinger 2014). We introduce some basic characteristics of our model below and refer interested readers to the aforementioned references for more details.

We start from an initial Gaussian realization of the density and velocity fields (Mesinger & Furlanetto 2007) in a large-volume (250 Mpc), grid-based, high-resolution ($\sim$0.65 Mpc; i.e. 250 Mpc/384) simulation box assuming periodic boundary conditions. These fields are then evolved according to second-order Lagrangian perturbation theory (Scoccimarro 1998), and regridded to a lower resolution ($\sim$1.95 Mpc; i.e. 250 Mpc/128) for the sake of computing efficiency. Then, for each cell centred at a spatial position and redshift of ($\mathbf{r}$, z), we compare the cumulative number per baryon of ionizing photons[7] ($\bar{n}_{\rm ion}$) to that of recombinations ($\bar{n}_{\rm rec}$) in spheres with decreasing radii (Furlanetto et al. 2004; Sobacchi & Mesinger 2014). A cell is ionized if at any radius R,

$$\bar{n}_{\rm ion} \geq (1 + \bar{n}_{\rm rec}). \tag{3}$$

Unresolved H II regions (smaller than the cell size) are accounted for according to Zahn et al. (2011).

The cumulative number of ionizing photons per baryon is obtained with

$$\bar{n}_{\rm ion}\left(\mathbf{r}, z | R, \delta_{R|\mathbf{r},z}\right) = \int {\rm d}M_{\rm vir} \phi\, f_{\rm duty}\, f_* \frac{\Omega_{\rm b}}{\Omega_{\rm m}} \frac{M_{\rm vir}}{\rho_{\rm b}} n_\gamma\, f_{\rm esc} \tag{4}$$

where $\delta_{R|\mathbf{r},z} \equiv \rho_{\rm b}/\bar{\rho}_{\rm b} - 1$ is the average overdensity within the spherical region, and $\rho_{\rm b}$ and $\bar{\rho}_{\rm b}$ represent the baryonic density and its cosmic mean. In equation (4)

(i) $M_{\rm vir}$ and $\phi\left(M_{\rm vir}, z | R, \delta_{R|\mathbf{r},z}\right)$ are the halo mass and halo mass function;

(ii) $f_{\rm duty}(M_{\rm vir}) = \exp(-\,M_{\rm turn}/M_{\rm vir})$, with a characteristic mass ($M_{\rm turn}$) as a free parameter, accounts for a decreasing occupation fraction of star-forming galaxies inside smaller haloes due to inefficient cooling, photoheating feedback (Efstathiou 1992; Shapiro,

---

[7]In this work, we do not consider ionization by X-ray photons or earlier objects such as minihalo-hosted galaxies, and their corresponding parameters. Although efficient at heating the IGM before reionization, X-rays, and minihaloes are expected to have a very minor contribution to the EoR for reasonable galaxy models (e.g. Ricotti & Ostriker 2004; McQuinn 2012; Mesinger, Ferrara & Spiegel 2013; Ross et al. 2017; Eide et al. 2018; Qin et al. 2020).

Giroux & Babul 1994; Thoul & Weinberg 1996; Hui & Gnedin 1997; Sobacchi & Mesinger 2013, 2014), or supernovae feedback (Wyithe & Loeb 2013; Hopkins et al. 2014, 2018; Mutch et al. 2016; Sun & Furlanetto 2016);

(iii) $f_*\left(M_{\rm vir}\right) = \min\left[1, f_{*,10}\left(M_{\rm vir}/10^{10}\,{\rm M}_\odot\right)^{\alpha_*}\right]$ is the fraction of galactic gas in stars and is assumed to scale with the host halo mass (Moster, Naab & White 2013; Mutch et al. 2016; Sun & Furlanetto 2016; Tacchella et al. 2018; Behroozi et al. 2019; Yung et al. 2019) according to the two free parameters, $f_{*,10}$ and α_*, representing the normalization and power-law index;

(iv) n_γ is the number of ionizing photons intrinsically emitted per stellar baryon; and

(v) $f_{\rm esc}\left(M_{\rm vir}\right) = \min\left[1, f_{\rm esc,10}\left(\frac{M_{\rm vir}}{10^{10}\,{\rm M}_\odot}\right)^{\alpha_{\rm esc}}\right]$ is the ionizing escape fraction defined as the number ratio of photons reaching the intergalactic medium (IGM) to those emitted in the galaxy, and is also assumed to scale with the halo mass (Ferrara & Loeb 2013; Kimm & Cen 2014; Paardekooper, Khochfar & Dalla Vecchia 2015; Xu et al. 2016).

Inside the H II regions, we estimate the local, average photoionization rate with (Sobacchi & Mesinger 2014)

$$\bar{\Gamma}_{\rm ion}\left(\mathbf{r}, z\right) = (1 + z)^2\, R \sigma_{\rm H} \frac{\alpha_{\rm UVB}}{\beta_{\rm H} + \alpha_{\rm UVB}} \frac{\bar{\rho}_{\rm b}}{m_{\rm p}} \dot{n}_{\rm ion}, \tag{5}$$

where $\sigma_{\rm H} = 6.3 \times 10^{-18}$ cm^2 and $\beta_{\rm H} \sim 2.75$ are the photoionization cross-section at Lyman limit and its spectral dependence; $\alpha_{\rm UVB} \sim 5$, $m_{\rm p}$, and $\dot{n}_{\rm ion}$ are the spectral indices of a stellar-driven UV ionizing background (Thoul & Weinberg 1996), the mass of a proton, and the local production rate of ionizing photons. Assuming the typical star formation time-scale is $t_* H^{-1}(z)$, with t_* being a free parameter, we calculate the average star formation rate (SFR) of galaxies in haloes of a given mass at a given redshift by

$$\text{SFR}\left(M_{\rm vir}, z\right) = \frac{M_*}{t_* H(z)^{-1}}, \tag{6}$$

convert it to the non-ionizing UV luminosity via $L_{1500}/\text{SFR} = 8.7 \times 10^{27}$erg s^{-1}Hz^{-1} M$_\odot^{-1}$yr (Madau & Dickinson 2014), and estimate $\dot{n}_{\rm ion}$ using equation (4) with M_* being replaced by the SFR.

We follow Sobacchi & Mesinger (2014) and estimate the recombination rate in each cell with a spatial position and redshift of ($\mathbf{r}$, z') as well as an overdensity of $\Delta_{\rm cell}$ by

$$\dot{n}_{\rm rec}\left(\mathbf{r}, z'\right) = \int {\rm d}\Delta_{\rm sub} \phi_{\rm sub} \alpha_{\rm B}\, f_{\rm H} \frac{\bar{\rho}_{\rm b}}{m_{\rm p}} \frac{\Delta_{\rm sub}^2}{\Delta_{\rm cell}} \left(1 - x_{\rm HI,sub}\right)^2. \tag{7}$$

Here, $\Delta_{\rm sub}$, $\phi_{\rm sub}(z', \Delta_{\rm sub}|\Delta_{\rm cell})$, $\alpha_{\rm B}$, $f_{\rm H}$, and $x_{\rm HI,sub}\left(z', \Delta_{\rm sub}, T_{\rm g}, \bar{\Gamma}_{\rm ion}\right)$ are the subgrid (unresolved) overdensity, its probability distribution function (PDF; e.g. Miralda-Escudé, Haehnelt & Rees 2000) within our large-scale simulation cell ($\sim$2 Mpc), case-B recombination coefficient evaluated at 10^4 K, number fraction of hydrogen in the universe, and the neutral hydrogen fraction of the subgrid gas element, respectively. We assume photoionization equilibrium in the ionized IGM, accounting for the attenuation of the local photoionization rate, $\bar{\Gamma}_{\rm ion}$, according to the radiative transfer simulations from Rahmati et al. (2013). We then compute the cumulative number of recombinations for each cell (see equation 3) by integrating $\dot{n}_{\rm rec}$ from the time the cell was ionized to the redshift of interest.

In summary, our model consists of the following six astrophysical parameters that we sample within the MCMC:

(i) $f_{*,10}$, the normalization of the stellar-to-galactic gas mass relation at $M_{\rm vir} = 10^{10}$ M$_\odot$, sampled with a flat prior in log space between 10^{-3} and 1;

(ii) α_*, the power-law index of the stellar-to-galactic gas mass relation, sampled with a flat prior between -0.5 and 1;

(iii) $f_{\rm esc, 10}$, the normalization of the ionizing escape fraction to halo mass relation at $M_{\rm vir} = 10^{10}\,{\rm M_\odot}$, sampled with a flat prior in log space between 10^{-3} and 1;

(iv) $\alpha_{\rm esc}$, the power-law index of the ionizing escape fraction to halo mass relation, sampled with a flat prior between -1 and 0.5;

(v) $M_{\rm turn}$, the turnover halo mass below which the number density of haloes hosting star-forming galaxies drops exponentially, sampled with a flat prior in log space between 10^8 and $10^{10}\,{\rm M_\odot}$;

(vi) t_*, the star formation time-scale as a fraction of the Hubble time, sampled with a flat prior between 0 and 1.

These prior ranges are chosen based on the physical meaning of the parameters. For example, fractions must range from 0 to 1, and we observe galaxies inside haloes with masses around $10^{10}\,{\rm M_\odot}$ thus setting an upper limit on $M_{\rm turn}$. More detailed discussion on the parameters and corresponding observational constraints can be found in Park et al. (2019).

We stress that our EoR model is both *flexible* and *physical*; both properties are important for useful inference. It is *flexible* in that it is capable of reproducing (see e.g. Park et al. 2019) the bulk properties and scalings of high-redshift galaxy observations (e.g. Bouwens et al. 2015, 2016; Oesch et al. 2018), as well as results from more sophisticated seminumerical models and hydrodynamic simulations (e.g. Mutch et al. 2016; Xu et al. 2016; Tacchella et al. 2018; Behroozi et al. 2019; Yung et al. 2019). It is *physical* in that the equations and parameters have a straightforward interpretation in terms of galaxy evolution, allowing us to set physically motivated priors for the free parameters.

For computational convenience, we fix the cosmology to the best-fitting values of *Planck* 2018 TT + low$E$ ($\Omega_{\rm m}$, $\Omega_{\rm b}$, Ω_Λ, h, σ_8 = 0.321, 0.04952, 0.679, 0.6688, 0.8118). In practice, one should covary astrophysical and cosmological parameters when performing inference. Fixing cosmological parameters effectively assumes that they are mostly constrained by the temperature and higher ℓ polarization PS (which are not considered in the likelihoods in this work), while the $\ell \leq 29$ E-mode PS constrains the EoR. There are less than 5 per cent differences ($< 1/3\,\sigma$) in the recovered optical depth from ignoring the temperature component in the likelihood. However, the most important degeneracy affecting the determination of $\tau_{\rm e}$ is the known '$A_s \exp(-2\tau_{\rm e})$' degeneracy (Planck Collaboration XLVI 2016d). Using the tan*h* model, we show in Appendix A that covarying σ_8 following that degeneracy has no impact on the reconstructed EoR history.

3.2 Hyperbolic tangent versus physically motivated EoR model

We perform MCMC simulations for the two different EoR models (tan*h* and 21CMFAST), both constrained using the low-ℓ EE PS. As an additional constraint, we also include the model-independent upper limit on the neutral hydrogen fraction at $z \sim 5.9$, $\bar{x}_{\rm HI} < 0.06 + 0.05(1\sigma)$, measured from the dark fraction in quasar spectra (McGreer, Mesinger & D'Odorico 2015) and modelling the associated likelihood as a one-sided Gaussian (Greig & Mesinger 2017a).

In Fig. 2, we show the resulting posterior for the tan*h* model using orange shaded regions, while the posterior corresponding to the astrophysical model is denoted with purple lines ([14, 86] and [2.3, 97.7] percentiles). The recovered EE PS, $\tau_{\rm e}$, and EoR history are shown clockwise from the top panel.

In the top panel, we see that the differences in the recovered PS are negligible between the two models. Neither model is able to recover

the excess power at $20 \lesssim \ell \lesssim 30$. However, the probability-to-exceed of these data as computed in Planck Collaboration V (2020a) points to a statistical fluctuation rather than a residual systematic error (or new physics not captured by our EoR modelling).

In the bottom right panel, we see that the distributions of $\tau_{\rm e}$ peak on similar scales, though the shape of the PDFs are qualitatively different. The recovered median and [14,86] percentiles are comparable (i.e. $\tau_{\rm e} = 0.0533^{+0.0078}_{-0.0068}$ for tan*h*; $\tau_{\rm e} = 0.0556^{+0.0080}_{-0.0064}$ for the astrophysical model). However, we note that the astrophysical model results in an asymmetric PDF of $\tau_{\rm e}$, with a tail extending towards high values.

The reason for this is apparent looking at the recovered EoR histories in the bottom left panel. The two distributions are comparable around the mid-point of reionization, where a large fraction of the EE power is imprinted. However, the astrophysical model (based on the growth of structure) results in asymmetric EoR histories with a tail towards higher redshifts. For example, at $z = 10$, the astrophysical model recovers $\bar{x}_{\rm HI} \gtrsim 0.849(1\sigma)$, while the tan*h* model recovers $\bar{x}_{\rm HI} \gtrsim 0.925(1\sigma)$. Thus, although the preference for a higher median optical depth is reduced in *Planck* 2018 compared to the 2015 data (see Section 2.1.1), the *natural shape* of the EoR history implied by the growth of structure does result in a (modest) high-redshift tail.

3.3 Optical depth versus power spectra

In the previous section, we discussed how inference from the *Planck* 2018 E-mode PS is affected by the choice of EoR models – tan*h* and astrophysical. In this section, we only use the astrophysical EoR model, and instead investigate the impact of the choice of likelihood statistic – using the EE PS directly versus using the $\tau_{\rm e}$ summary statistic. In addition to the choice of CMB statistics, we also account for the (model independent) upper limit on the neutral hydrogen fraction at $z \sim 5.9$ from the dark fraction in quasar spectra (McGreer et al. 2015) as well as the galaxy UV LFs at $z = 6 - 10$ from Bouwens et al. (2015, 2016) and Oesch et al. (2018); both of these independent data sets are included as priors in the total likelihood, as described in Park et al. (2019).

In Fig. 3, we show the marginalized posteriors for the astrophysical parameters (panels in *lower left corner*), together with the corresponding: (1) EE PS; (2) EoR history; and (3) $\tau_{\rm e}$ (*upper right*). We run three different MCMC simulations corresponding to different combinations of observational data sets used for the likelihood:

(i) *DarkFraction_LF*, including high-redshift LFs and the quasar dark fraction upper limit on $\bar{x}_{\rm HI}(z = 5.9)$. This run does not consider any CMB observations;

(ii) *DarkFraction_tau_LF*, based on *DarkFraction_LF*, but including an additional constraint on $\tau_{\rm e} = 0.0522 \pm 0.0080$, which is taken from the TT + low$E$ reconstruction in *Planck* 2018 (Planck Collaboration VI 2020b) and was generated using a tan*h* basis set; and

(iii) *DarkFraction_EE_LF*, based on *DarkFraction_LF*, but also forward-modelling the low-ℓ E-mode PS using CLASS (Lesgourgues 2011) and includes the low-ℓ EE likelihood from *Planck* 2018 (Planck Collaboration V 2020a). These are our 'flagship' constraints.

Looking at the posterior of *DarkFraction_LF*, we see that some of our astrophysical parameters are already constrained by galaxy and quasar observations. As pointed out in Park et al. (2019) (see also e.g. Tacchella et al. 2018; Behroozi et al. 2019; Yung et al. 2019), the observed high-redshift UV LFs already constrain the SFR-to-halo mass relation to within factors of ~ 2 (i.e. $f_{*, 10}/t_*$ and α_*) and provide an upper limit on the characteristic halo mass below which
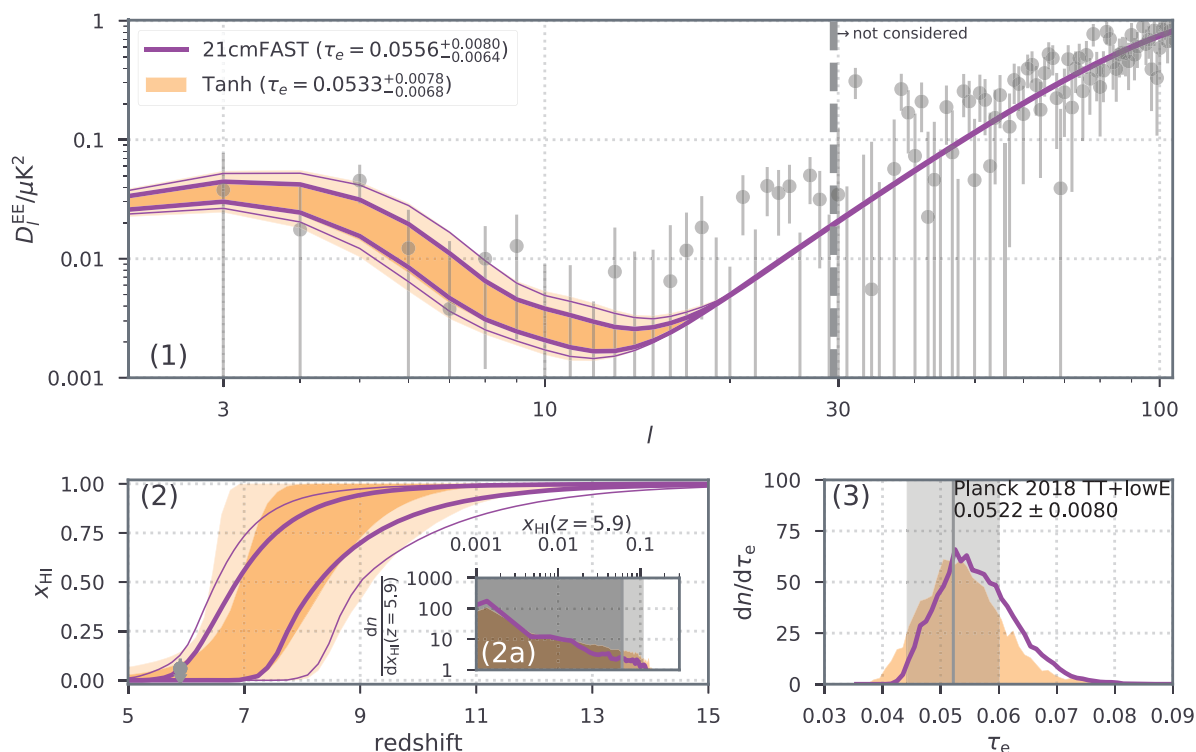
Figure 2. Posteriors of our astrophysical EoR model (*purple*) and the tan*h* EoR model (*orange*), recovered from the E-mode polarization PS on large scales ($2 \leq \ell \leq 29$; Planck Collaboration V 2020a; grey circles shown in panel 1) and the upper limit on the neutral hydrogen fraction at $z \sim 5.9$ (McGreer et al. 2015; grey shaded regions shown in panel 2a). The 14–86 (2.3–97.7) percentiles of (1) the E-mode polarization PS and (2) the mean neutral hydrogen fraction evolution in the posteriors are presented using thick (thin) lines or dark (light) shaded regions. PDFs of (2a) the neutral hydrogen fraction at $z = 5.9$ and (3) the Thompson optical depth are also shown for the two MCMC results. Although, the recovered PS and τ_e are comparable between the two models, the astrophysical model (based on the hierarchical structural growth) results in asymmetric EoR histories with tails towards high redshifts.

the galaxy occupancy fraction starts decreasing ($M_{\rm turn} \lesssim 10^{9.5}\,{\rm M_\odot}$; 2σ). Additionally, the dark fraction measurement of quasar spectra sets a lower limit for the ionizing escape fraction normalization ($f_{\rm esc, 10} > 0.02$; 2σ), requiring the bulk of reionization to occur before $z \sim 6$ (panel 2) and setting a lower limit on τ_e (panel 3). However, without the CMB, the early stages of reionization are unconstrained (cf. Greig & Mesinger 2017a). This is evident from the broad range of EoR histories allowed beyond $z \gtrsim 8$ (panel 2), as well as the broad distributions of τ_e (panel 3) and the PS (panel 1). These early EoR models generally correspond to the high $f_{\rm esc}$ + low $\alpha_{\rm esc}$ corner of astrophysical parameter space.[8]

Including CMB observations rules out early reionizing models. Both *DarkFraction_tau_LF* and *DarkFraction_EE_LF* posteriors disfavour the high $f_{\rm esc}$ and low $\alpha_{\rm esc}$ corner of parameter space. The EE PS, EoR history, and τ_e distributions all shrink.

Comparing the *DarkFraction_tau_LF* and *DarkFraction_EE_LF* posteriors in Fig. 3 quantifies the bias of using the τ_e summary statistic, generated with a different EoR model, instead of directly

forward-modelling the CMB PS. There is a small difference in the EE PS with *DarkFraction_EE_LF* allowing for a slightly earlier EoR. In general, however, the two posteriors are nearly identical. This indicates that, with the *Planck* 2018 data, the bias in using τ_e for the likelihood instead of the EE PS directly is negligible.

Finally, Fig. 4 presents the constrained photonionization rate ($\Gamma_{\rm ion}$; see equation 5). This serves to further illustrate how a physical model allows us to predict additional IGM properties. We only show *DarkFraction_tau_LF*, as *DarkFraction_EE_LF* is nearly identical, while not including the CMB observations allows $\Gamma_{\rm ion}$ to become unrealistically large. The rise in $\Gamma_{\rm ion}$ with redshift is determined by the formation of structure in our galaxy model, with the 'flattening' seen at $z \lesssim 6$–7 being due to photoheating suppression of gas accretion on to galaxies following reionization (e.g. Sobacchi & Mesinger 2013). We see that while our prediction is consistent with the measured UV ionizing background at $z \sim 5$ to 6 (Bolton & Haehnelt 2007; Calverley et al. 2011; Wyithe & Bolton 2011), observational data lie on the lower boundary. Additionally including $z \sim 5$–6 Lyα transmission statistics constrains the upper envelope of $\Gamma_{\rm ion}$ significantly, though the results are more model dependent than those presented here (Qin et al., in preparation).

We should caution, however, that our findings here are valid in the context of a flat ΛCDM universe. An important follow-up to this study will be to generalize these trends to alternative cosmologies (e.g. Paoletti et al. 2020). It is possible that in some exotic cosmologies, the correlation between parameters describing exotic physics and reionization exist at the level of τ_e but are broken once the full power of the CMB PS is included, rendering the necessity of joint analysis of reionization data and CMB observations.

---

[8]We note that if our prior ranges were extended even further, reionization would be allowed at even higher redshifts. However, an important benefit of using an astrophysical EoR model is that it allows us to place physically motivated priors on the parameters. For example, an ionizing escape fraction cannot be higher than unity, nor can star formation occur efficiently inside haloes whose virial temperature is smaller than available gas cooling channels. This is not the case for non-physical or so-called model-independent constraints, for which it can be difficult to choose reasonable priors on the model parameters.
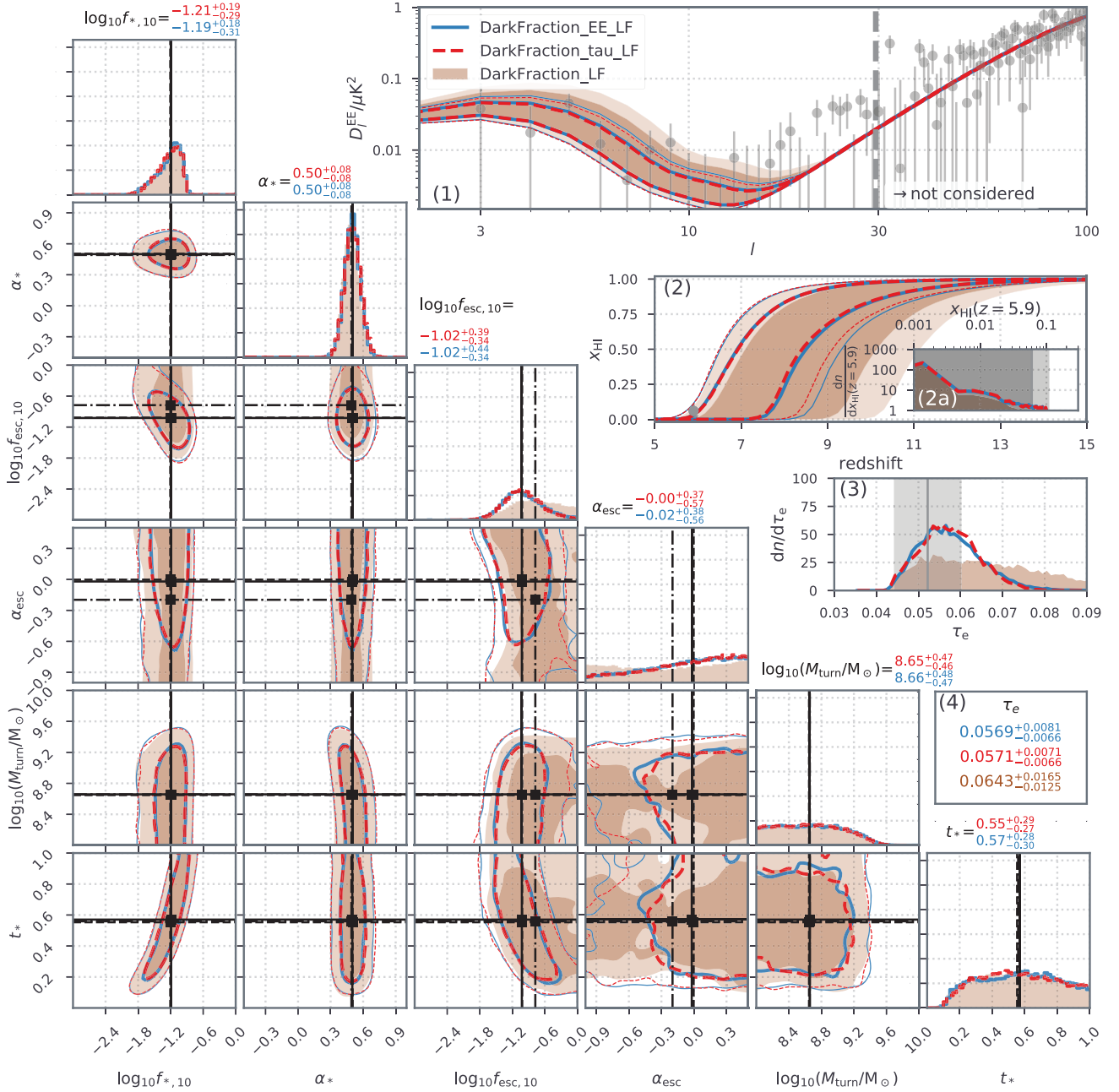
Figure 3. Marginalized posterior distributions of the astrophysical model parameters with different observational constraints: (i) *DarkFraction_LF* (brown shaded regions) uses high-redshift LFs and the quasar dark fraction measurements; (ii) *DarkFraction_tau_LF* (red dashed lines) uses high-redshift LFs, the quasar dark fraction measurements, and τ_e derived using a tan*h* EoR model; and (iii) *DarkFraction_EE_LF* (blue solid lines) uses high-redshift LFs, the quasar dark fraction measurements, and the low-ℓ EE PS. The 2D distributions correspond to 68th (dark regions or thick lines) and 95th (light regions or thin lines) percentiles. The upper right three subpanels present the [14, 86] (and [2.3, 97.7]) percentiles of (1) the E-mode polarization PS and (2) evolution of the mean neutral hydrogen fraction ($\bar{x}_{\rm HI}$), as well as the PDFs of (2a) $x_{\rm HI}$ at $z = 5.9$ and (3) the Thompson scattering optical depth. The median and [14, 86] percentiles of the inferred optical depth are presented in the lower right box (4). Observational constraints are indicated in grey. Overall, we see *insignificant difference* in the posteriors between *DarkFraction_tau_LF* and *DarkFraction_EE_LF*, indicating a negligible bias in inference when using the τ_e summary statistic generated with a different EoR basis set (instead of directly forward-modelling the EE PS).

4 CONCLUSIONS

In this work, we develop an interface between 21CMFAST and CLASS, allowing us to forward-model the large-scale E-mode polarization power spectra inside the 21CMMC sampler. With this set-up, we study how the choice of (i) EoR model (astrophysical versus a tan*h*) and (ii) likelihood statistic (τ_e versus EE PS), impacts EoR parameter inference.

The marginalized posteriors of τ_e for the *Planck* 2018 data (Planck Collaboration V 2020a) are fairly insensitive to the parametrization of the EoR history: tan*h* versus a galaxy model. This is contrary to claims based on the earlier 2015 release (e.g. Miranda et al. 2017; Millea & Bouchet 2018; Planck Collaboration VI 2020b; Hazra et al. 2020). However, the galaxy model (based on standard hierarchical growth of structure) results in asymmetric EoR histories, with the
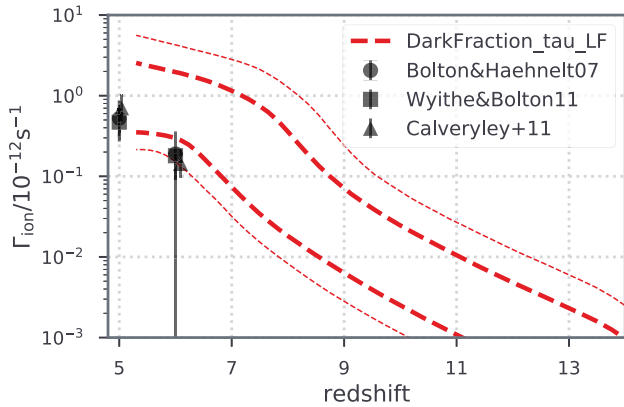
Figure 4. The [14, 86] (and [2.3, 97.7]) percentiles of the photoionization rate from models used in the *DarkFraction_tau_LF* posterior in Fig. 3. Observational constraints (Bolton & Haehnelt 2007; Calverley et al. 2011; Wyithe & Bolton 2011) are indicated in grey.

early stages extending to higher redshifts (see also Choudhury & Ferrara 2006; Wise et al. 2014; Price, Trac & Cen 2016; Qin et al. 2017; Gorce et al. 2018; Kulkarni et al. 2019). As a result, the lower limit on the volume averaged neutral hydrogen fraction at $z = 10$ changes from $\bar{x}_{\rm HI} \gtrsim 0.93(1\sigma)$ using the tan*h* model to $\bar{x}_{\rm HI} \gtrsim 0.85(1\sigma)$ using an astrophysical model.

Using our galaxy EoR model, we quantify the bias in inference when the likelihood is computed from the $\tau_{\rm e}$ summary statistic, compared with directly using the measured E-mode polarization PS. We perform MCMC simulations taking into account the current observational constraints from high-redshift galaxy UV LFs (Bouwens et al. 2015, 2016; Oesch et al. 2018) and the model-independent constraints from the dark fraction in quasar spectra (McGreer et al. 2015). Additionally including either CMB statistic helps constrain the posterior, ruling out models that have a high escape fraction for faint galaxies and hence an early reionization. However, the difference between using $\tau_{\rm e}$ for the likelihood, compared with the EE PS, is negligible. Our flagship constraints, based on the quasar dark fraction + UV LFs + EE PS, result in an optical depth of $\tau_{\rm e} = 0.0569^{+0.0081}_{-0.0066}(1\sigma)$, with asymmetric EoR histories.

DATA AVAILABILITY

The data underlying this article will be shared on reasonable request to the corresponding author.

REFERENCES

Behroozi P., Wechsler R. H., Hearin A. P., Conroy C., 2019, MNRAS, 488, 3143
Bolton J. S., Haehnelt M. G., 2007, MNRAS, 382, 325
Bouwens R. J. et al., 2015, ApJ, 803, 34
Bouwens R. J. et al., 2016, ApJ, 830, 67
Calverley A. P., Becker G. D., Haehnelt M. G., Bolton J. S., 2011, MNRAS, 412, 2543
Chluba J., 2010, MNRAS, 402, 1195
Choudhury T. R., Ferrara A., 2006, MNRAS, 371, L55
Douspis M., Aghanim N., Ilić S., Langer M., 2015, A&A, 580, L4
Dvorkin C., Hu W., Smith K. M., 2009, Phys. Rev. D, 79, 107302
Efstathiou G., 1992, MNRAS, 256, 43P
Eide M. B., Graziani L., Ciardi B., Feng Y., Kakiichi K., Di Matteo T., 2018, MNRAS, 476, 1174
Ferrara A., Loeb A., 2013, MNRAS, 431, 2826
Furlanetto S. R., Zaldarriaga M., Hernquist L., 2004, ApJ, 613, 1
Gorce A., Douspis M., Aghanim N., Langer M., 2018, A&A, 616, A113
Greig B., Mesinger A., 2015, MNRAS, 449, 4246
Greig B., Mesinger A., 2017a, MNRAS, 465, 4838
Greig B., Mesinger A., 2017b, MNRAS, 472, 2651
Hazra D. K., Paoletti D., Finelli F., Smoot G. F., 2020, Phys. Rev. Lett., 125, 071301
Heinrich C., Hu W., 2018, Phys. Rev. D, 98, 063514
Heinrich C. H., Miranda V., Hu W., 2017, Phys. Rev. D, 95, 023513
Hogan C. J., Anderson S. F., Rugers M. H., 1997, AJ, 113, 1495
Hopkins P. F., Kereš D., Oñorbe J., Faucher-Giguère C.-A., Quataert E., Murray N., Bullock J. S., 2014, MNRAS, 445, 581
Hopkins P. F. et al., 2018, MNRAS, 480, 800
Hu W., 2000, ApJ, 529, 12
Hu W., Dodelson S., 2002, ARA&A, 40, 171
Hu W., Holder G. P., 2003, Phys. Rev. D, 68, 023001
Hui L., Gnedin N. Y., 1997, MNRAS, 292, 27
Kimm T., Cen R., 2014, ApJ, 788, 121
Koh D., Wise J. H., 2018, MNRAS, 474, 3817
Kulkarni G., Keating L. C., Haehnelt M. G., Bosman S. E. I., Puchwein E., Chardin J., Aubert D., 2019, MNRAS, 485, L24
Lesgourgues J., 2011, preprint (arXiv:1104.2932)
Lewis A., 2008, Phys. Rev. D, 78, 023002
Madau P., Dickinson M., 2014, ARA&A, 52, 415
McGreer I. D., Mesinger A., D'Odorico V., 2015, MNRAS, 447, 499
McQuinn M., 2012, MNRAS, 426, 1349
McQuinn M., Furlanetto S. R., Hernquist L., Zahn O., Zaldarriaga M., 2005, ApJ, 630, 643
Mesinger A., Furlanetto S., 2007, ApJ, 669, 663
Mesinger A., Furlanetto S., Cen R., 2011, MNRAS, 411, 955
Mesinger A., Ferrara A., Spiegel D. S., 2013, MNRAS, 431, 621
Millea M., Bouchet F., 2018, A&A, 617, A96
Miralda-Escudé J., Haehnelt M., Rees M. J., 2000, ApJ, 530, 1
Miranda V., Lidz A., Heinrich C. H., Hu W., 2017, MNRAS, 467, 4050
Mortonson M. J., Hu W., 2008, ApJ, 672, 737
Moster B. P., Naab T., White S. D. M., 2013, MNRAS, 428, 3121
Mutch S. J., Geil P. M., Poole G. B., Angel P. W., Duffy A. R., Mesinger A., Wyithe J. S. B., 2016, MNRAS, 462, 250
Oesch P. A., Bouwens R. J., Illingworth G. D., Labbé I., Stefanon M., 2018, ApJ, 855, 105
Paardekooper J.-P., Khochfar S., Dalla Vecchia C., 2015, MNRAS, 451, 2544
Page L. et al., 2007, ApJS, 170, 335
Paoletti D., Hazra D. K., Finelli F., Smoot G. F., 2020, J. Cosmol. Astropart. Phys., 09, 005
Park J., Mesinger A., Greig B., Gillet N., 2019, MNRAS, 484, 933
Planck Collaboration XI, 2016a, A&A, 594, A11
Planck Collaboration XIII, 2016b, A&A, 594, A13
Planck Collaboration XVI, 2016c, A&A, 594, A16
Planck Collaboration XLVI, 2016d, A&A, 596, A107
Planck Collaboration XLVII, 2016e, A&A, 596, A108
Planck Collaboration V, 2020a, A&A, 641, A5
Planck Collaboration VI, 2020b, A&A, 641, A6
Price L. C., Trac H., Cen R., 2016, preprint (arXiv:1605.03970)
Qin Y. et al., 2017, MNRAS, 472, 2009
Qin Y., Mesinger A., Park J., Greig B., Muñoz J. B., 2020, MNRAS, 495, 123

Rahmati A., Pawlik A. H., Raičević M., Schaye J., 2013, MNRAS, 430, 2427

Raskutti S., Bolton J. S., Wyithe J. S. B., Becker G. D., 2012, MNRAS, 421, 1969

Reichardt C. L., 2016, in Mesinger A., ed., Astrophysics and Space Science Library, Vol. 423, Observing the Epoch of Reionization with the Cosmic Microwave Background. Springer-Verlag, Berlin, p. 227

Ricotti M., Ostriker J. P., 2004, MNRAS, 352, 547

Ross H. E., Dixon K. L., Iliev I. T., Mellema G., 2017, MNRAS, 468, 3785

Roy A., Lapi A., Spergel D., Baccigalupi C., 2018, J. Cosmol. Astropart. Phys., 2018, 014

Scoccimarro R., 1998, MNRAS, 299, 1097

Seager S., Sasselov D. D., Scott D., 1999, ApJ, 523, L1

Shapiro P. R., Giroux M. L., Babul A., 1994, ApJ, 427, 25

Sobacchi E., Mesinger A., 2013, MNRAS, 432, L51

Sobacchi E., Mesinger A., 2014, MNRAS, 440, 1662

Spergel D. N. et al., 2007, ApJS, 170, 377

Sun G., Furlanetto S. R., 2016, MNRAS, 460, 417

Sunyaev R. A., Zeldovich I. B., 1980, MNRAS, 190, 413

Tacchella S., Bose S., Conroy C., Eisenstein D. J., Johnson B. D., 2018, ApJ, 868, 92

Thoul A. A., Weinberg D. H., 1996, ApJ, 465, 608

Vishniac E. T., 1987, ApJ, 322, 597

Wise J. H., Demchenko V. G., Halicek M. T., Norman M. L., Turk M. J., Abel T., Smith B. D., 2014, MNRAS, 442, 2560

Worseck G. et al., 2011, ApJ, 733, L24

Worseck G., Prochaska J. X., Hennawi J. F., McQuinn M., 2016, ApJ, 825, 144

Wyithe J. S. B., Bolton J. S., 2011, MNRAS, 412, 1926

Wyithe J. S. B., Loeb A., 2013, MNRAS, 428, 2741

Xu H., Wise J. H., Norman M. L., Ahn K., O'Shea B. W., 2016, ApJ, 833, 84

Yung L. Y. A., Somerville R. S., Popping G., Finkelstein S. L., Ferguson H. C., Davé R., 2019, MNRAS, 490, 2855

Zahn O., Mesinger A., McQuinn M., Trac H., Cen R., Hernquist L. E., 2011, MNRAS, 414, 727

APPENDIX A: RECONSTRUCTED EOR WHEN COVARYING σ_8

It is well known that there exists a strong degeneracy between the optical depth to reionization τ_e and the amplitude of the primordial power spectrum A_s in the high-ℓ ($\ell \gtrsim 30$) TT, TE, EE power spectrum, such that the parameter combination well-constrained by these data is $A_s \exp(-2\tau_e)$ (Planck Collaboration XLVI 2016d). Once the physical densities $\Omega_m h^2$, $\Omega_b h^2$ and the tilt of the primordial power spectrum n_s are fixed, there is a direct correspondence between A_s and σ_8, and hence σ_8 inherits this degeneracy with τ_e. As a result, one might worry that fixing σ_8, as we have done for computational convenience, would overconstrain the optical depth and the EoR reconstructed from the low-ℓ PS.

To test this, in Fig. A1 we plot the analogous quantities from Fig. 2, using the tan$h$ parametrization, which is much less time-consuming than 21CMFAST. In orange, we show the same model as in Fig. 2, generated by fixing σ_8. In blue, we show the posterior of the tan$h$ model, but also allowing σ_8 to covary with a prior on the $\sigma - \tau_e$ relation inherited from the high-multipole data (see fig. 42 and discussion in Planck Collaboration XLVI 2016d). The fact that the orange and blue posteriors are virtually indistinguishable suggests that our conclusions are unaffected by our choice of fixing cosmological parameters while performing inference.
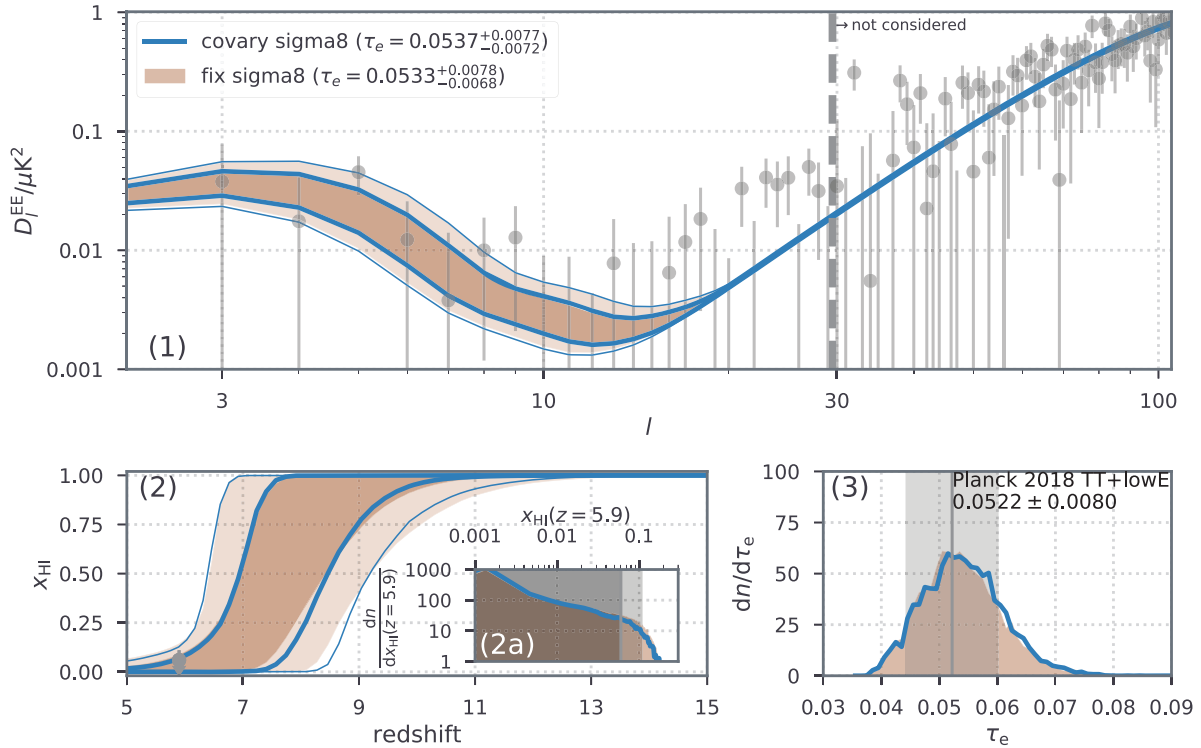

Figure A1. Same as Fig. 2, but for the tan$h$ EoR model with (*blue*) and without covarying σ_8 (*orange*). For the posterior shown in blue, we put a prior on the $\sigma_8 - \tau_e$ relation inferred from the high-ℓ data (see fig. 42 in Planck Collaboration XLVI 2016d). The difference between the two results is negligible.

This paper has been typeset from a T$_{\rm E}$X/L^{A}T$_{\rm E}$X file prepared by the author.